This article has been accepted for publication in a future issue of this journal, but has not been fully edited. Content may change prior to final publication. Citation information: DOI 10.1109/TMECH.2015.2494842, IEEE/ASME Transactions on Mechatronics

Cardioscopic Tool-delivery Instrument for Beating-heart Surgery

Asghar Ataollahi, Ignacio Berra, Nikolay V. Vasilyev, Zurab Machaidze and Pierre E. Dupont, *Fellow, IEEE*

***Abstract*—This paper describes an instrument that provides solutions to two open challenges in beating-heart intracardiac surgery - providing high-fidelity imaging of tool-tissue contact and controlling tool penetration into tissue over the cardiac cycle. Tool delivery is illustrated in the context of tissue removal for which these challenges equate to visualization of the tissue as it is being removed and to control of cutting depth. Cardioscopic imaging is provided by a camera and illumination system encased in an optical window. When the optical window is pressed against tissue, it displaces the blood between the camera and tissue allowing clear visualization. Control of cutting depth is achieved via precise extension of the cutting tool from a port in the optical window. Successful tool use is demonstrated in ex vivo and in vivo experiments.**

I. Introduction

Repairs inside the heart are performed either by open surgery or via catheter. While surgery involves substantial trauma and requires placing the patient on cardiopulmonary bypass, catheter-based procedures are much lower risk and often do not even require general anesthesia. Furthermore, the number of procedures that can be performed via catheter is growing. These include transcatheter aortic valve replacement [1] and catheter-delivered clips to reduce or eliminate mitral valve regurgitation [2]. Despite these advances, there are still many procedures that can only be performed by open surgery.

An important example in pediatrics is to correct ventricular stenosis caused by excess tissue in the outflow tracts of the ventricles [3]. Similarly, in adults, surgical tissue removal is used to treat hypertrophic cardiomyopathy [4]. In these procedures, several cubic centimeters of tissue must be removed.

There are several challenges to converting procedures such as tissue removal to beating-heart interventions. First, millimeter-resolution imaging is often needed to ensure that a tool is positioned at the desired location on the heart wall. In valve repair, for example, a device may need to be placed a fixed number of millimeters from the free edge of a leaflet. For tissue removal, there is a need to visualize both the tissue to be removed as well as to inspect the region where tissue has been removed.

The standard imaging modalities available in a catheterization lab are fluoroscopy and ultrasound. While fluoroscopy provides the desired resolution with respect to the catheter, it does not image soft tissue. Ultrasound provides visualization of both the catheter and the tissue, however, the images are noisy and imaging artifacts from the catheter can obscure the adjacent tissue.

This work was supported by the the NIH under grant R01HL124020. Thanks to S. Berra for development of the pulsatile pump system. A. Ataollahi, I. Berra, N. Vasilyev, Z. Machaidze and P. Dupont are with Cardiovascular Surgery, Boston Children's Hospital, Harvard Medical School, Boston, MA, 02115, USA. {first.last}@childrens.harvard.edu.

Optical imaging offers the potential to augment fluoroscopic and ultrasound imaging by providing intuitive local images of the intervention site. The challenge of optical imaging inside the heart, however, is seeing through the blood. Three approaches have been attempted to overcome this challenge: infrared imaging [5], [6], continuous flushing with clear liquid [7] and use of an optical window [8], [9]. In the latter, a transparent optical window is pressed against the tissue to displace the blood, providing a clear and detailed view of the contacting tissue. The advantages of the optical window are that it provides excellent image quality in comparison to infrared and does not require continuous fluid injection into the bloodstream.

A second challenge to performing beating-heart interventions is that stabilization of a tool with respect to the beating heart is necessary to enable task performance and to avoid accidental damage of sensitive heart structures or perforation of the heart wall. In this context, the inherent compliance of catheters designed for safe navigation of the vasculature proves to be an impediment to tool-tissue stabilization.

One approach to stabilization is to move the tool to match the motion of the cardiac tissue. It has been shown, however, that human motion tracking is limited to frequencies of 1Hz or less [10],[11]. Given normal cardiac frequencies of 1-1.67Hz, manual tracking of a heart motion is not possible. To overcome this limitation, robotic systems have been developed in which sensors measure tissue motion and automatically servo the tool so as to cancel the relative motion or to maintain a desired contact force [12], [13].

While elegant, robotic solutions adds substantial cost and complexity. An inexpensive alternative to moving a tool in synchrony with the tissue is to press against the tissue so as to locally immobilize it with respect to the tool. While the high stiffness of a handheld instrument facilitates this approach, the challenge is that the contact force needed for stabilization can greatly exceed the desired tool-tissue contact force. It can also result in overpenetration of the tool into the tissue.

In the tissue removal task, for example, local immobilization performed using the tool itself could easily result in perforation of the heart wall. Consequently, published results on beating heart tissue removal have been limited to creation of an atrial septal defect consisting of a hole between the right and left atria [14]. This procedure did not require precise depth control since the goal was penetration of the tissue layer. Furthermore, this procedure did not require high-resolution imaging since the hole can be located anywhere in the central region of the 3cm wide septum.

The contribution of this paper is to provide an integrated solution to the challenges of imaging and tool-tissue stabilization. Imaging is achieved using a camera encased in an optical window (Fig. 1). The contact between the optical window

This article has been accepted for publication in a future issue of this journal, but has not been fully edited. Content may change prior to final publication. Citation information: DOI 10.1109/TMECH.2015.2494842, IEEE/ASME Transactions on Mechatronics

and the tissue is employed for dual purposes. It displaces the blood for visualization while also applying the force needed for local tissue immobilization. Tools are deployed through a working channel in the optical window. In this way, tool-tissue interaction can be controlled independently of tissue immobilization. At the same time, tool-tissue contact can also be visualized. In the context of tissue removal, cutting depth is controlled by the extension of the cutting tool from the surface of the optical window, which acts as the equivalent of the sole plate of a woodworking router.

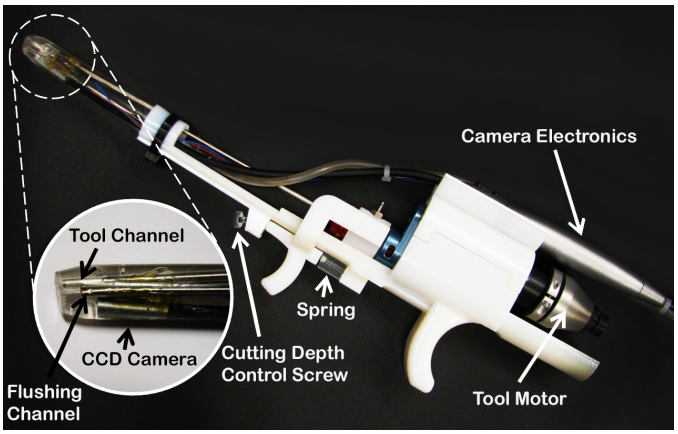

Fig. 1. Handheld instrument for cardioscopically-guided tissue removal.

While catheter deployment is the ultimate goal, the approach is demonstrated here in the context of a handheld tool inserted through the heart wall. Image-guided procedures using tools inserted through the wall of the beating heart represent a middle ground between surgery on a stopped heart and transcatheter interventions and have been proposed and demonstrated for a variety of procedures [15], [8], [16].

The remainder of the paper is arranged as follows. Section II describes design and integration of the handheld system. Section III provides ex vivo and in vivo experimental validation of the approach. Section IV presents conclusions and indicates future directions.

II. Instrument Design

The endoscopic instrument of Fig. 1 consists of three main components: a tissue removal tool, an imaging system and lightweight handle providing trigger-based control of tool extension. The tissue removal tool is mounted at the tip of a straight tube and is driven by a rotating inner tube powered by a motor as shown. The imaging system is comprised of an optically clear window with an integrated 5mm diameter VGA 640×480 resolution 30 fps CMOS video camera and LED illumination. The optical window provides a channel for controlled insertion of the tissue removal tool as well as a second channel for flushing the window-tissue interface. The handle is designed to integrate the endoscope and the tool into a single instrument for ease of operation and to provide precise control of tool extension into tissue. Each component is detailed in the following subsections.

A. Tissue removal tool

The tissue removal tool as depicted in Fig. 2 has a diameter of 2mm. It is manufactured using a metal MEMS (MicroElectoMechanical Systems) fabrication process in which 25μm thick layers of structural (NiCo) and sacrificial metal (Cu) are deposited using a photolithographic electrodeposition process [14]. The design can be easily scaled in diameter and consists of two parts, a stator and rotor, which are attached by an integrated bearing.The rotor is laser welded to an inner motor-driven rotating tube while the stator attaches by a snap fit to a stationary outer tube. A vacuum pump is used to create aspiration of cutting debris through the rotating tube. To avoid clogging as well as excessive blood loss, the cutting interface is irrigated with heparinized saline supplied in the clearance between the tubes.

The stator possesses two cutting windows. Efficient tissue removal occurs when the tool is oriented such that tissue presses against one of the cutting windows. The meshing teeth of the rotor and stator slice the tissue and, ideally, all debris is transported out through the aspiration channel. Prior work has shown that sliding the tool across the tissue surface at an orientation of about 45° with respect to the tissue surface normal provides the best results [14].

In similarity to a machining operation, the depth of cut during each pass over the tissue must be limited to avoid gouging the tissue or damaging the tool. Heart tissue motion over the cardiac cycle varies by location, but can be up to a centimeter. Consequently, depth of cut cannot be controlled simply by rigid positioning of the cutting tool since the tool will plunge in and out of the tissue as the heart beats. The approach used here is to locally immobilize the tissue with respect to the optical window by pressing the window against the tissue. Then, by controlling extension of the cutting tool from the optical window, the depth of cut into the tissue can be independently controlled. This issue is addressed further in Section II-C on handheld tool design.

B. Imaging system

The imaging system consists of a camera and illumination source contained in an optical window that also incorporates a tool channel and flushing port. This system differs from a standard endoscope in that the optical window must be designed to displace blood when pressed against tissue inside the beating heart. Tool-tissue interaction is then visualized through the optical window. Furthermore, the working channel and flushing port must be self-sealing to avoid the accidental injection of air into the heart or loss of blood out of the heart [17].

Based on these design constraints, we created a transparent optical window with an integrated 5 mm diameter CMOS camera and LED illumination. Figure 3 shows the final cardioscope design. It is fabricated using a transparent RTV-2 silicone rubber material (QSil 216, Quantum Silicones LLC) by casting inside a custom designed polymer mold. Rather than design the device with a separate optical window and body, use of a transparent silicone enables the molding of a one-piece design incorporating a tubular camera, tool channel and saline

This article has been accepted for publication in a future issue of this journal, but has not been fully edited. Content may change prior to final publication. Citation information: DOI 10.1109/TMECH.2015.2494842, IEEE/ASME Transactions on Mechatronics

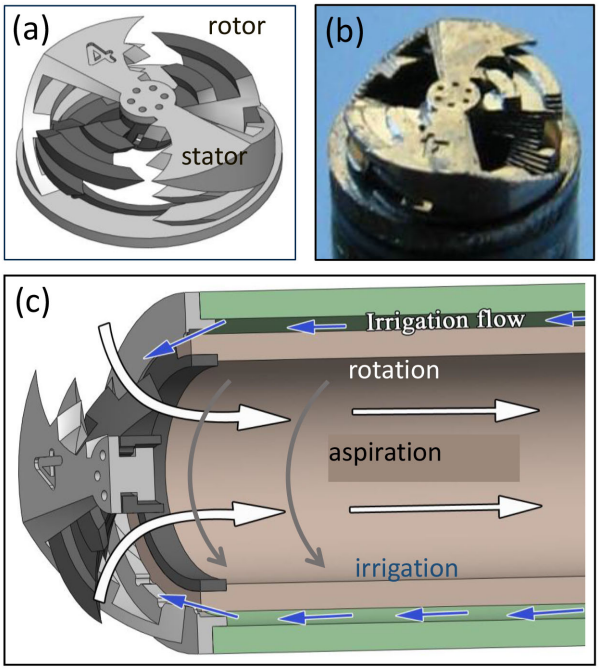

Fig. 2. Tissue removal tool fabricated using a metal MEMS process. (a) Schematic illustrating rotor and stator. (b) Actual device with 2mm diameter. (c) Drive system showing irrigation and aspiration channels.

injection channel. This approach simplifies fabrication and eliminates the optical distortion that would occur due to any interfaces between the camera lens and the face of the optical window. Medical-grade silicone is widely available and is used for interventional tools as well as implantable devices.

The tool channel is lined with a 2.15mm inner diameter stainless steel tube that ends 10mm from the face of the optical window. The tube serves to reduce friction between the tool and the silicone channel ensuring that small forces are needed to adjust depth of cut. The distal 10mm section has a diameter of 1.9mm to ensure its sealing around the tissue removal tool.

The saline injection channel is designed for clearing the view in the case when some blood is trapped between the window and the tissue. In addition, when the window is not in tissue contact, it is possible to displace the blood in front of the window by ejecting a bolus of saline. This temporarily enables visualization of structures located a few millimeters in front of the window. This feature facilitates safe navigation towards the target tissue prior to physical contact. The flushing channel is located behind the tool channel and camera in the view of Figure 3 to avoid occluding the tool view. It is comprised of a stainless steel tube that ends 5mm from the face of the optical window, outside the view of the camera. The distal end of the flushing channel is self sealing due to the flexibility of the silicone rubber material.

The following procedural specifications were used to design the geometry of the optical window as well as the relative orientation between the tissue removal tool and the camera.

1) Maximize the field of view on the tissue,
2) Provide visualization of tissue both before and after removal within the field of view,
3) Optimize the angle of tool-tissue contact, and

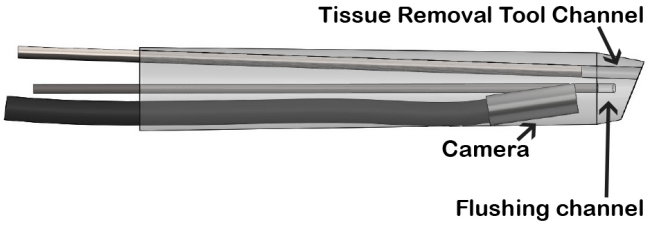

Fig. 3. Single-piece cardioscope design molded from transparent silicone.

4) Accommodate angle of tool approach specified by a surgical procedure

A variety of optical window shapes, as shown in Fig. 4, were considered. The hemispherical design of Fig. 4 facilitates the displacement of blood during tissue contact. Furthermore, the tissue removal tool can be positioned off center, as shown, to achieve the optimal tool-tissue cutting angle of 45°. Its nominal field of view in tissue contact consists of one point, however, which also fails to meet the visualization criteria, (2). As a specific example, when a 12mm diameter hemispherical optical window is pressed against ex vivo tissue using only the weight of the tool itself, the diameter of the contact region is about 9mm. Note that the actual field of view can be smaller than the contact region depending on camera positioning and aspect ratio. While the field of view can be increased by pressing the instrument into the tissue with greater force, this deformation interferes with the controlled sliding of the instrument over the tissue during the tissue removal process.

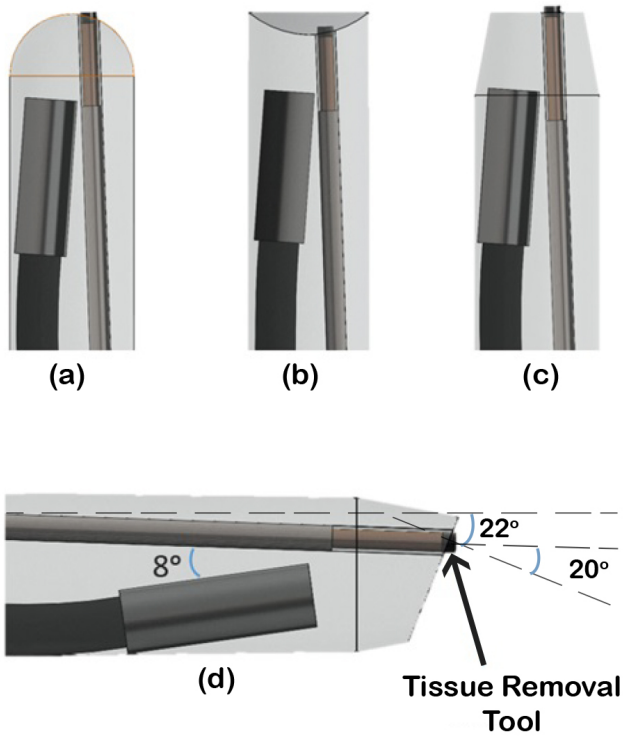

Fig. 4. Optical window design. (a) Convex design,(b) Concave design, (c) Flat-surface design, (d) The optimized angled flat-surface design.

To avoid these problems, the designs of Fig. 4(b) and (c)

This article has been accepted for publication in a future issue of this journal, but has not been fully edited. Content may change prior to final publication. Citation information: DOI 10.1109/TMECH.2015.2494842, IEEE/ASME Transactions on Mechatronics

were considered. In Fig. 4(b), surface curvature is reduced to a single axis. To investigate this design, a 12.7mm diameter semi-cylindrical optical window was considered. With a nominal field of view comprising a line contact, the contact region enlarges to be approximately rectangular and about 8×12.7mm in size when pressed against ex vivo tissue using only the weight of the tool itself.

The planar surface of Fig. 4(c) provides the largest field of view at minimum contact force - the contact region consists of a circle of the same diameter as the window face. In addition, in testing with cardiac tissue, it was found that the planar surface was still effective at evacuating blood during tissue contact. Furthermore, the planar design allows the tissue removal tool to be positioned in the field of view to satisfy specification (2).

While the planar design depicted in Fig. 4(c) fails to satisfy the tool-tissue contact angle criteria (3), it is necessary to simultaneously satisfy criteria (4). For this study, the instrument was designed to perform tissue removal in the outflow tract of the right ventricle. The desired configuration of the instrument during the surgical procedure is illustrated in Fig. 5. The instrument is inserted through the right ventricular free wall to remove excess tissue in the funnel-shaped infundibulum. While it is not possible from a single insertion point to remove tissue around the entire outflow tract, a sufficient portion of the infundibulum is accessible from this entry point. From the figure, it can be observed that the angle between the instrument axis and the tissue normal varies over the range of approximately 0-45°.

As confirmed with the depicted 3D heart model as well as ex vivo pig hearts, a planar window angled between 20-25° from the axis of the cardioscope enabled the best overall window contact over the entire region targeted for tissue removal. While hearts differ in size, variations can be accommodated by slightly changing the insertion location and via compliance of the heart wall at the point of insertion. As shown in Fig. 4(d), an angle of 22° was selected in the final design.

Ex vivo experiments also revealed that as the diameter of the planar window increased, it became more difficult to slide the instrument over the tissue. In addition, there was an increased tendency for blood to be trapped between the planar window and the nonplanar and, in some locations, nonsmooth tissue surface. Consequently, the instrument diameter tapers from 14mm, where it passes through the heart wall, to 10mm at the face of the optical window. This value provides a compromise between a large field of view and smooth instrument-tissue motion.

While it might appear that criteria 2 would be best satisfied by positioning the tool channel in the center of the optical window, this not optimal for two reasons. First, the procedure requires tissue removal in the corners under the valve. (Note that the valve is cut away in Fig. 5 for instrument visualization.) Consequently, the tool channel must be positioned close (2mm) to the sharp edge of the optical window. Second, the camera and tool channel need to be angled toward each other to visualize cutting and to observe the depth of cut. The 14mm instrument diameter accommodates a relative angle of 8°, which is achieved by rotating the camera by 6° and the tool channel by 2°. The resulting tool-tissue angle of 20° is less than the optimal angle of 45°, but still large enough for effective cutting. This configuration results in a camera field of view of 7.5×10mm.

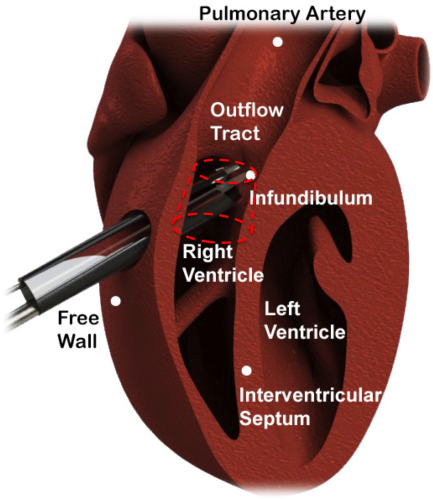

Fig. 5. Tool inserted through free wall of right ventricle to remove excess tissue in the funnel-shaped outflow tract (infundibulum, marked with dashed red line) below pulmonary valve.

C. Handheld tool design

The goal of the design process was to create an instrument that a surgeon could easily position and slide on the tissue surface. Furthermore, it should enable the operator to independently control the tissue contact force, for localized tissue stabilization, and the penetration depth of the tool into the tissue. The latter is accomplished by controlling extension of the tissue removal tool from the optical window.

Two generations of tools were designed and tested. The first generation is shown in Fig. 6 while the second generation appears in Fig. 1. The first generation design used a standard clinical endoscope (Olympus A5257A 5mm, 0° laparoscope; Smith & Nephew 460H CCD camera, 768×494 NTSC). The endoscope, tissue removal tool and optical window are integrated by means of a lightweight handle fabricated by 3D printing from ABS (Acrylonitrile Butadiene Styrene) plastic. The design incorporates a trigger for controlling extension of the cutting tool from the optical window. Initially, the cutting tool is retracted inside the endoscope. As the trigger handle is squeezed, the tool extends from the optical window a distance proportional to the squeeze displacement. A set screw is used to limit maximum extension.

The first generation design, as evaluated through ex vivo and in vivo testing, was found to have three shortcomings. The most important limitation arose from its 740g mass as well as its mass distribution. The camera (not shown) and the proximal end of the endoscope comprised 315g of the total – creating a top-heavy mass distribution. This made it difficult to position and slide the optical window on the cardiac tissue. This motivated us to replace the endoscope with the lightweight CMOS camera in the second generation design.

This article has been accepted for publication in a future issue of this journal, but has not been fully edited. Content may change prior to final publication. Citation information: DOI 10.1109/TMECH.2015.2494842, IEEE/ASME Transactions on Mechatronics

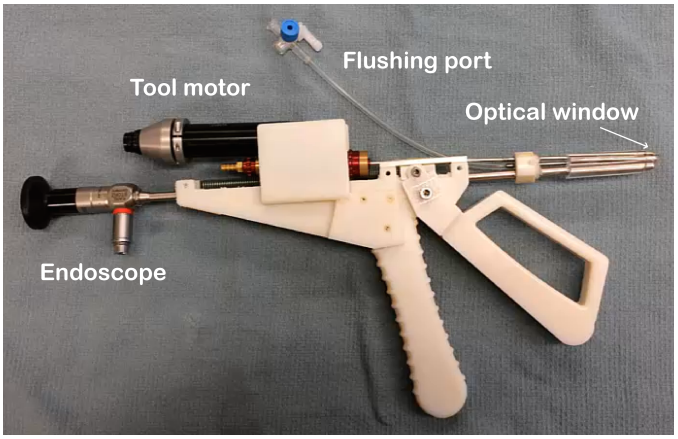

Fig. 6. First generation design employing standard endoscope for imaging.

The second and third limitations arose due to the design of the handle and trigger. The size of the handles was found to necessitate a much larger incision than otherwise would be necessary. Furthermore, as described in the next section, the best cutting is achieved by specific submillimeter extensions of the tool from the optical window. It was not possible for the operator to accurately control tool extension via relative motion of the handles.

To eliminate these shortcomings, two changes were made in the design of the second-generation device. First, the handle and trigger were replaced with low-profile finger grips and moved toward the proximal end of the instrument as shown in Fig. 1. Second, the trigger mechanism was modified. Since the desired tool extension is a fraction of a millimeter, the new trigger is operated in an on-off fashion. When pulled, the cutting tool is fully retracted into the optical window. When released, a spring extends the tool from the window by a specific submillimeter distance that has been set in advance using an adjusting screw. With these modifications, the second-generation design, shown in Fig. 1, has a mass of 370g making it easy to position and control using one hand.

III. Experimental Evaluation

Two types of experiments were performed to evaluate the second-generation instrument in the context of tissue removal in the outflow tract of the right ventricle. The instrument design described above was used for both experiments. Porcine hearts were used owing to their anatomical and geometric similarity to the human heart. The first set of experiments were performed on ex vivo hearts connected to a pulsatile pumping system. These experiments were used to obtain experience with the instrument and to verify the appropriate cutting speed and depth of cut. Subsequently, an in vivo experiment was conducted to validate the approach under surgical conditions. Each is described below.

A. Ex vivo pulsatile heart model

Ex vivo experiments were performed using hearts acquired at a local slaughterhouse. A pulsatile pumping system was used to pump saline in and out of the ventricle through the vasculature and so mimic natural cardiac motion. The instrument entered the free wall of the right ventricle as depicted in Fig. 5.

Tissue removal requires both control of cutting depth as well as control of tool motion over the tissue surface. To determine if the tissue removal could be constrained to a specific area of the surface despite pulsatile motion, a waterproof blue pen was used to demark a 15mm diameter circle on the infundibulum as shown in Fig. 7(a).

The instrument was inserted through an incision in the free wall of the right ventricle and a purse string suture was used to seal the opening around the instrument (Fig. 7(b)). This incision location as well as the purse string suture technique replicate standard surgical procedure. Note that the sutures shown in Fig. 7(b) were placed by our surgeon (IB) to repair tissue slices made by the slaughterhouse.

The tissue to be removed consists of two layers. The endocardium is the thin elastic layer lining the inside of the heart. It is more difficult to cut and tends to tear off in patches that can jam the tissue removal tool. The myocardium lying beneath it is more easily cut into small pieces. Prior to pulsatile testing, tissue from 3 hearts was used to determine that the fastest tissue removal technique that also avoided tool jamming. It was found that removing tissue on a layer by layer basis provided the best results.

To remove the endocardium, the trigger-controlled cutting depth was set to 0.3mm and the tool rotational speed was set to 1000RPM. This resulted in the generation of small pieces of endocardium and so avoided tool jamming. After removing endocardial tissue in the region of interest, the cutting depth was increased to 0.8mm and tool speed was decreased to 600RPM. This combination of cutting depth and tool speed resulted in the fastest rate of myocardial tissue removal.

Tissue removal was performed by a pediatric cardiac surgeon (second author). Figs. 7(c) and (d) illustrate the results of endocardial and myocardial tissue removal, respectively. Note how the cardioscopic view enabled the operator to limit tissue removal to the marked region. As an extreme test of tissue removal, cutting was performed to an average depth of 10mm, which is deeper than a typical procedure would require. The total tissue volume removed was approximately 0.7cm^3 and was performed in 6 minutes, 25 seconds. Based on the success of this experiment and the satisfaction of the surgeon with the instrument, it was decided to proceed directly to in vivo testing.

B. In vivo experiment

An in vivo experiment was performed on an anesthetized 65kg swine. To match the tissue removal performed for subvalvular stenosis, tissue was removed in two regions of the infundibulum. The instrument was inserted through a small incision in the right ventricle free wall and sealed with a purse string suture as shown in Fig. 8. Stabilization is entirely due to contact between the instrument and the heart.

Cardioscopic imaging inside the beating heart was first evaluated as shown in Fig. 9. Fig. 9(a) depicts the view in the blood-filled heart prior to tissue contact. The saline

This article has been accepted for publication in a future issue of this journal, but has not been fully edited. Content may change prior to final publication. Citation information: DOI 10.1109/TMECH.2015.2494842, IEEE/ASME Transactions on Mechatronics

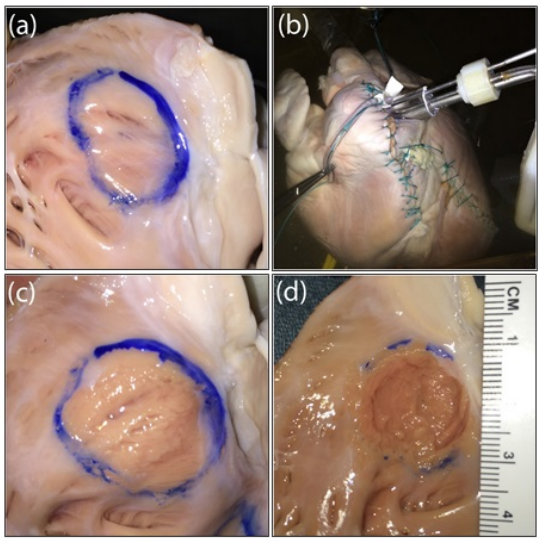

Fig. 7. Beating heart ex-vivo experiment: (a) Marked region of interest, (b) Tool insertion port through the right ventricular free wall, (c) Endocardial tissue removal, (d) Myocardial tissue removal.

injection port was then tested. As shown in Fig. 9(b), when the instrument is near the heart wall, the saline can flush the blood from in front of the optical window to temporarily provide a clear view of the adjacent tissue.

Endocardial tissue removal was next performed using settings of 0.3 mm for depth of cut and 1000 RPM for tool speed. Figs. 9(c) and (d) illustrate imaging during removal of the endocardium. The wide field of view assists in determining the region of contact and provides detailed visual feedback on the progress of cutting. After removing endocardium in the desired regions, the depth of cut was set to 0.8 mm and tool speed was reduced to 600RPM. Intraoperative imaging of myocardial tissue removal is depicted in Figs. 9(e) and (f).

Tissue removal proceeded until the surgeon judged that the outflow tract of the pulmonary valve had been sufficiently enlarged and that an amount of tissue, comparable to that of a pediatric procedure, had been removed. The procedure was well tolerated by the animal. After completing tissue removal, the animal was sacrificed and the heart was examined. As shown in Fig. 10, the heart has been cut open for visualization of the outflow tract. The two regions of tissue removal measure 16×10mm and 20×7mm and vary in depth up to 6mm.

The approximate volume of tissue removed was 0.9cm^3, about 28% more than in the ex vivo experiment. The amount and location of tissue removed matched the surgeon's goals. Furthermore, a total tissue removal time of 3 minutes 23 seconds was deemed to be extremely fast compared to an open procedure. The speed of removal compared to that of ex vivo tissue is likely due to the difference in tissue properties between live and dead tissue.

Irrigation and aspiration of the tissue removal tool were monitored during the procedure. The total irrigation volume of heparinized saline was 210ml while the volume of aspirated liquid was 130ml. Hematocrit tests comparing a blood sample with the aspirated liquid indicated that only 8ml of the aspirated liquid was blood with the remainder corresponding to irrigation fluid. This suggests that the optical window is effective in minimizing the aspiration of blood.

To evaluate entrapment of tissue debris, the aspirated liquid was filtered using a 40 micron cell strainer (BD Falcon). The debris was examined under a microscope and weighed. The largest pieces of tissue debris were less than 3 mm long. The total debris was less than 39mg, however, indicating that a significant amount of debris escaped into the bloodstream. This issue needs further study prior to human testing. One potential solution is the use of an embolic filter inserted in the pulmonary artery during the procedure.

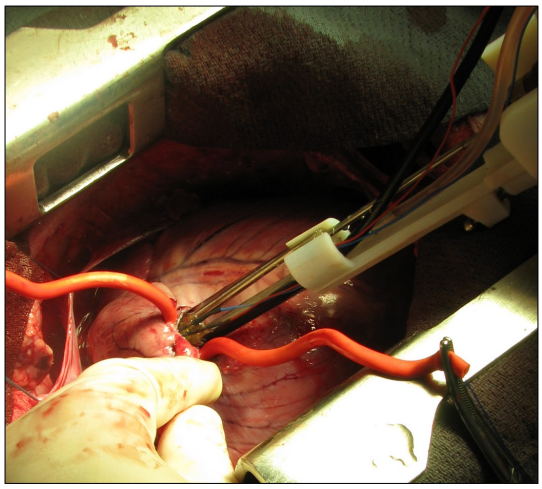

Fig. 8. Cardioscopic instrument inserted into the beating heart of a swine.

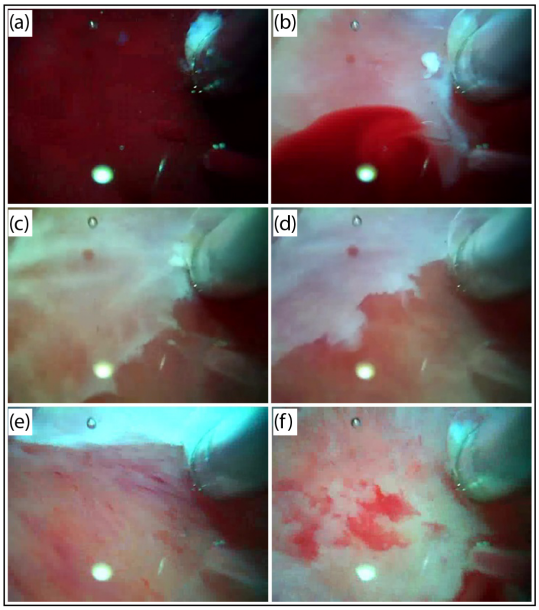

Fig. 9. In vivo cardioscopic view. (a) View of blood prior to tissue contact. (b) Temporary view of nearby non-contacting tissue after blood-clearing saline injection. (c),(d) Removal of endocardium. Endocardium remains in upper left, but has been removed in lower right. (e),(f) Removal of myocardium. Note in (f) tendency of myocardium to fragment.

This article has been accepted for publication in a future issue of this journal, but has not been fully edited. Content may change prior to final publication. Citation information: DOI 10.1109/TMECH.2015.2494842, IEEE/ASME Transactions on Mechatronics

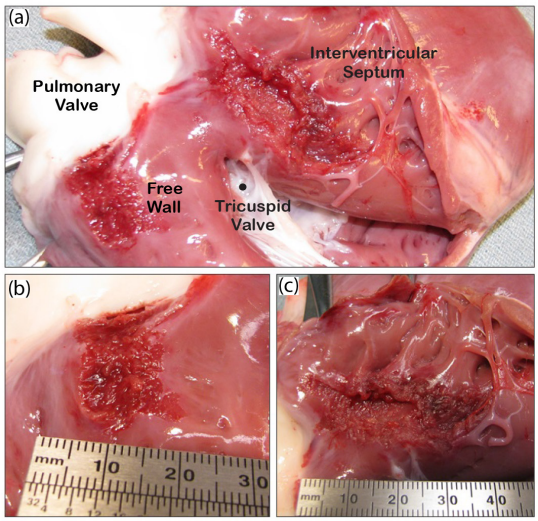

Fig. 10. Postsurgical evaluation of tissue removal. (a) Right ventricle has been opened to show two regions in outflow tract where tissue was removed. (b) Closeup of left region. (c) Closeup of right region.

IV. Conclusions

The results of this paper indicate that cardioscopic imaging inside the beating heart can be a valuable modality for solving the dual challenges of tool-tissue visualization and stabilization. The optical window is employed not only for imaging, but also to apply the force needed for local immobilization of the tissue with respect to the tool. Tool-tissue contact is mediated independently using a trigger mechanism to control tool extension from the optical window in sub-millimeter increments. This technique could be beneficial both for improving existing beating-heart interventions as well as for enabling new procedures.

In the context of tissue removal, which is among the most challenging beating-heart procedures, we have demonstrated imaging quality that greatly exceeds what is currently provided by ultrasound imaging. Furthermore, we have shown qualitatively that cutting depth can be controlled in both ex vivo and in vivo experiments.

An additional feature is the saline injection port that provides the capability to temporarily clear the blood in front of the optical window - providing a clear view of nearby tissue. This feature can aid in the visualization of uneven surfaces, e.g., trabeculated tissue, and could also facilitate safe navigation inside the heart by avoiding contact with sensitive structures.

The single-piece molded silicone design is simple and inexpensive to fabricate and represents an attractive solution for transcardiac beating-heart tissue removal. Current research is investigating a miniature version of this design mounted at the tip of a robotic catheter.

References

[1] S. Kodali, M. Williams, C. Smith, L. Svensson, J. Webb, R. Makkar, G. Fontana, T. Dewey, V. Thourani, A. Pichard, M. Fischbein, W. Szeto, S. Lim, K. Greason, P. Teirstein, S. Malaisrie, P. Douglas, R. Hahn, B. Whisenant, A. Zajarias, D. Wang, J. Akin, W. Anderson, and M. P. T. I. Leon, "Two-year outcomes after transcatheter or surgical aortic-valve replacement," *N Engl J Med.*, vol. 366, no. 18, pp. 1686–95, 2012.

[2] L. Mauri, E. Foster, D. Glower, P. Apruzzese, J. Massaro, H. Herrmann, J. Hermiller, W. Gray, A. Wang, W. Pedersen, T. Bajwa, J. Lasala, R. Low, P. Grayburn, and T. E. I. I. Feldman, "4-year results of a randomized controlled trial of percutaneous repair versus surgery for mitral regurgitation," *J Am Coll Cardiol.*, vol. 62, no. 4, pp. 317–28, 2013.

[3] J. Aboulhosn and J. Child, "Left ventricular outflow obstruction: subaortic stenosis, bicuspid aortic valve, supravalvar aortic stenosis, and coarctation of the aorta," *Circulation*, vol. 114, no. 22, pp. 2412–22, 2006.

[4] P. M. Elliott, A. Anastasakis, M. A. Borger, M. Borggrefe, F. Cecchi, P. Charron, A. A. Hagege, A. Lafont, G. Limongelli, H. Mahrholdt, W. J. McKenna, J. Mogensen, P. Nihoyannopoulos, S. Nistri, P. G. Pieper, B. Pieske, C. Rapezzi, F. H. Rutten, C. Tillmanns, and H. Watkins, "2014 esc guidelines on diagnosis and management of hypertrophic cardiomyopathy," *European Heart Journal*, 2014.

[5] B. P. Knight, M. C. Burke, T. E. Hong, A. McAuley, D. Amundson, J. Hanlin, L. Blankenship, T. B. F. Jr., S. Nazarian, and R. D. Berger, "Direct imaging of transvenous radiofrequency cardiac ablation using a steerable fiberoptic infrared endoscope," *Heart Rhythm*, vol. 2, no. 10, pp. 1116 – 1121, 2005.

[6] W. S. Grundfest, J. Val-Mejias, E. Monnet, B. P. Knight, S. Nazarian, R. D. Berger, T. B. F. Jr, M. M. Roden, D. Amundson, J. Hanlin, and L. Blankenship, "Real-time percutaneous optical imaging of anatomical structures in the heart through blood using a catheter-based infrared imaging system," *Seminars in Thoracic and Cardiovascular Surgery*, vol. 19, no. 4, pp. 336 – 341, 2007.

[7] Y. Uchida, "Recent advances in percutaneous cardioscopy," *Current Cardiovascular Imaging Reports*, vol. 4, no. 4, pp. 317–327, 2011.

[8] N. V. Vasilyev, J. F. Martinez, F. P. Freudenthal, Y. Suematsu, G. R. Marx, and P. J. del Nido, "Three-dimensional echo and videocardioscopy-guided atrial septal defect closure," *The Annals of Thoracic Surgery*, no. 4, pp. 1322–1326, 2006.

[9] M. Padala, J. H. Jimenez, A. P. Yoganathan, A. Chin, and V. H. Thourani, "Transapical beating heart cardioscopy technique for off-pump visualization of heart valves," *The Journal of Thoracic and Cardiovascular Surgery*, vol. 144, no. 1, pp. 231 – 234, 2012.

[10] V. Falk, "Manual control and tracking a human factor analysis relevant for beating heart surgery," *The Annals of Thoracic Surgery*, vol. 74, no. 2, pp. 624–628, 2002.

[11] S. Jacobs, D. Holzhey, B. B. Kiaii, J. F. Onnasch, T. Walther, F. W. Mohr, and V. Falk, "Limitations for manual and telemanipulator-assisted motion trackingimplications for endoscopic beating-heart surgery," *The Annals of Thoracic Surgery*, vol. 76, no. 6, pp. 2029 – 2035, 2003.

[12] S. G. Yuen, N. V. Vasilyev, P. J. del Nido, and R. D. Howe, "Robotic tissue tracking for beating heart mitral valve surgery," *Medical image analysis*, vol. 17, pp. 1236–1242, 12 2013.

[13] E. E. Tuna, J. H. Karimov, T. Liu, . Bebek, K. Fukamachi, and M. C. avuolu, "Towards active tracking of beating heart motion in the presence of arrhythmia for robotic assisted beating heart surgery," *PLoS ONE*, vol. 9, p. e102877, 07 2014.

[14] N. V. Vasilyev, A. H. Gosline, A. Veeramani, M. T. Wu, G. P. Schmitz, R. T. Chen, V. Arabagi, P. J. del Nido, and P. E. Dupont, "Tissue removal inside the beating heart using a robotically delivered metal mems tool," *The International Journal of Robotics Research*, vol. 34, no. 2, pp. 236–247, 2015.

[15] Y. Suematsu, J. Martinez, B. Wolf, G. Marx, J. Stoll, P. Dupont, R. Howe, J. Triedman, and P. del Nido, "Beating-heart patch closure of muscular ventricular septal defects under real-time 3d echo guidance: A pre-clinical study," *Journal of Thoracic and Cardiovascular Surgery*, vol. 130, no. 5, pp. 1348–57, 2005.

[16] N. Vasilyev, I. Melnychenko, K. Kitahori, F. Freudenthal, A. Phillips, R. Kozlik-Feldmann, and E. A. Bacha, "Beating-heart patch closure of muscular ventricular septal defects under real-time 3d echo guidance: A pre-clinical study," *Journal of Thoracic and Cardiovascular Surgery*, vol. 135, no. 3, pp. 603–609, 2008.

[17] N. Vasilyev, M. Kawata, C. DiBiasio, K. Durand, J. Hopkins, Z. Traina, A. Slocum, and P. del Nido, "A novel cardioport for beating-heart image-guided intracardiac surgery," *Journal of Thoracic and Cardiovascular Surgery*, vol. 142, no. 6, pp. 1545–51, 2011.